

Galaxy Science with ORCAS: Faint Star-Forming Clumps to $AB \lesssim 31$ mag and $r_e \gtrsim 0''.01$ ROGIER A. WINDHORST,¹ TIMOTHY CARLETON,¹ SETH H COHEN,¹ ROLF JANSEN,¹ ROSALIA O'BRIEN,¹ SCOTT TOMPKINS,¹
DANIEL COE,² JOSE M. DIEGO,³ AND BRIAN WELCH⁴¹*School of Earth and Space Exploration, Arizona State University, Tempe, AZ 85287-1404*²*Space Telescope Science Institute, 3700 San Martin Drive, Baltimore, MD 21218*³*IFCA, Instituto de Fisica de Cantabria (UC-CSIC), Avenida de Los Castros s/n, 39005 Santander, Spain*⁴*Center for Astrophysical Sciences, Department of Physics and Astronomy, The Johns Hopkins University, 3400 N Charles St., Baltimore, MD 21218*

Abstract

The NASA concept mission ORCAS (“Orbiting Configurable Artificial Star”) aims to provide near diffraction-limited angular resolution at visible and near-infra-red wavelengths using laser signals from space-based cubesats as Adaptive Optics beacons for ground-based 8–30 meter telescopes, in particular the 10 meter Keck Telescopes. When built as designed, ORCAS+Keck would deliver images of $\sim 0''.01$ – $0''.02$ FWHM at 0.5–1.2 μm wavelength that reach $AB \lesssim 31$ mag for point sources in a few hours over a $\gtrsim 5 \times 5''$ FOV that includes IFU capabilities. We summarize the potential of high-resolution faint galaxy science with ORCAS. We show that the ability to detect optical–near-IR point sources with $r_e \gtrsim 0''.01$ FWHM to $AB \lesssim 31$ mag will yield about 5.0×10^6 faint star-forming (SF) clumps per square degree, or ~ 0.4 per arcsec², or one in every box of $1.6 \times 1.6''$. From recent HST lensing data, the typical *intrinsic* (*i.e.*, *unlensed*) sizes of SF clumps at $z \simeq 1$ – 7 will be $r_e \simeq 1$ – 80 m.a.s. to $AB \lesssim 31$ mag, with *intrinsic* (*i.e.*, *unmagnified*) fluxes as faint as $AB \lesssim 35$ – 36 mag when searching with ORCAS around the critical curves of the best lensing clusters imaged with HST and JWST. About half of these SF clumps will have sizes below the ORCAS diffraction limit, and the other half will be slightly resolved, but still mostly above the ORCAS surface brightness (SB) limits. A $\gtrsim 5 \times 5''$ ORCAS FOV may therefore provide just enough compact SF clumps to do relative m.a.s.-astrometry. ORCAS will address how galaxies assemble from smaller clumps to stable disks by measuring ages, metallicities, and gradients of clumps within galaxies. Of particular interest will be to follow up with ORCAS on caustic transits of individual stars in SF clumps at $z \gtrsim 1$ – 2 that have been detected with HST, and those that may be detected with JWST at $z \simeq 6$ – 17 at extreme magnifications ($\mu \gtrsim 10^3$ – 10^5) for the first stars and their stellar mass black hole accretion disks. The ability of ORCAS to monitor such stars for decades across the (micro-)caustics provides a unique opportunity to obtain a statistical census of individual stars at cosmological distances, leveraging the largest telescope apertures that are available only on the ground.

Keywords: Galaxies: Galaxy Counts — Galaxies: Sizes — Gravitational Lensing: Clump Sizes — Gravitational Lensing: Caustic Transits

1. INTRODUCTION

In the last three decades, major progress has been made in studies of galaxy assembly with the Hubble Space Telescope (HST) and through targeted programs using Adaptive Optics (AO) on the world’s best ground-based facilities. It is not possible to review all these efforts here, and so we refer the reader to more detailed reviews (*e.g.*, Livio et al. 1998; Cristiani et al. 2001; Mather et al. 2006; Ellerbroek et al. 2006; Gardner et al. 2006). In Windhorst et al. (2008), we reviewed the advantages of high resolution science on high redshift galaxies from the ground as compared to from space. In short, diffraction limited space-based imaging provides much darker sky over a wider FOV, more stable PSF’s, better dynamic range, and therefore superior sensitivity, including in the vacuum-UV. But ground-based

multi-conjugate AO (MCAO) on 8-10 meter telescopes is *complementary* to space-based imaging, as it can provide much higher spatial resolution — and spectral resolution — than what space-based telescopes can currently do.

One of the early discoveries by HST was that the numerous faint blue galaxies are in majority late-type (*e.g.*, Abraham et al. 1996; Driver et al. 1995, 1998; Glazebrook et al. 1995, and references therein) and small (Odewahn et al. 1996; Cohen et al. 2003; Hathi et al. 2008, see Fig.2 here) star-forming objects. These are the building blocks of the giant galaxies seen today (*e.g.*, Pascarelle et al. 1996). By measuring their distribution over rest-frame type (Windhorst et al. 2002) versus redshift, HST has shown that galaxies of all Hubble types formed over a wide range of cosmic time, but with a notable transition around redshifts $z \simeq 0.5\text{--}1.0$ (*e.g.*, Driver et al. 1995, 1998; Elmegreen et al. 2007). This was done through HST programs like, *e.g.*, the Medium-Deep Survey (Griffiths et al. 1994), the Hubble Deep Field (HDF Williams et al. 1996), GOODS (Giavalisco et al. 2004), GEMS (Rix et al. 2004), the Hubble UltraDeep Field (HUDF Beckwith et al. 2006), COSMOS (Scoville et al. 2007), and CANDELS (Grogin et al. 2011; Koekemoer et al. 2011). Coupled with models of galaxy formation, these observations suggest that subgalactic units rapidly merged from the end of reionization (Bouwens et al. 2004a; Yan et al. 2004b) to grow bigger units at lower redshifts (*e.g.*, Pascarelle et al. 1996). Merger products start to settle as galaxies with giant bulges or large disks around redshifts $z \simeq 1$ (*e.g.*, Lilly et al. 1998, 2007). These have evolved mostly passively since then, resulting in giant galaxies today (*e.g.*, Driver et al. 1998; Cohen et al. 2003).

Star-forming clumps have also been studied at high resolution in lower redshift turbulent galactic disks (*e.g.*, Fisher et al. 2017a,b). The size evolution of star-forming galaxies has been studied out to $z \lesssim 7$ (*e.g.*, Ferguson et al. 2004; Allen et al. 2017), where galaxy half-light or effective radii r_e approximately decrease with redshift as $r_e(z) \propto r_e(0) \cdot (1+z)^{-s}$ with $s \simeq 0.9\text{--}1.2$. This strong size evolution reflects the hierarchical formation of galaxies, where sub-galactic clumps and smaller galaxies merge over time to form the larger/massive galaxies that we see today (*e.g.*, Navarro et al. 1996). It was the reason that HST was so successful after its refurbishment in December 1993 at identifying faint compact star-forming galaxies that form hierarchically at $z \simeq 1\text{--}7$ in the Λ CDM universe. The compact object sizes thereby helped to mitigate the enormous $(1+z)^4$ cosmological SB-dimming that would quickly render large extended objects undetectable at higher redshifts (*e.g.*, Windhorst et al. 2008).

The combination of ORCAS (“Orbiting Configurable Artificial Star”; <https://asd.gsfc.nasa.gov/orcas/>) cube sat laser MCAO beacons with ground-based 8–39 meter telescopes has the great potential to provide nearly diffraction limited imaging over wider FOV’s than possible with AO alone. For instance, ORCAS combined with the 10 meter Keck telescope can provide PSF FWHM values $\lesssim 0''.01\text{--}0''.02$ (10–20 mas) at $0.5\text{--}1.25 \mu\text{m}$ wavelength, and still provide a sufficient FOV ($5 \times 5''\text{--}10 \times 10''$) to detect a significant number of objects to very faint fluxes ($AB \lesssim 31$ mag). In the optical–near-IR, ORCAS+Keck can thus compete with space-based imaging in terms of increased spatial resolution, low sky-brightness in its very small pixels, and therefore increased point source sensitivity. In the thermal infrared ($\lambda \gtrsim 2 \mu\text{m}$), for which JWST was designed and optimized (Gardner et al. 2006), space-based imaging will remain superior in terms of PSF-stability, sky-brightness, depth, and FOV.

2. THE SURFACE DENSITY OF FAINT STAR-FORMING CLUMPS TO $AB \lesssim 31$ MAG FOR ORCAS

For the success of ORCAS galaxy science, we need to be able to accurately estimate the expected number density of faint compact star-forming objects out to $z \lesssim 7$ and $AB \lesssim 31$ mag. To interpret the currently available lensed samples of SF clumps, we also need to make an estimate of the *intrinsic* object counts anticipated to $AB \lesssim 35\text{--}36$ mag. The deepest available data to date are summarized in Fig 1a-1b for the HST ACS/WFC F606W (wide V-band) and WFC/IR F125W (J-band) filters or their ground-based equivalents. These data came from the panchromatic ground-based GAMA survey (which covers $AB \lesssim 18$ mag; Driver et al. 2011), the panchromatic HST WFC ERS survey ($17 \lesssim AB \lesssim 26.5$ mag; Windhorst et al. 2011), and the panchromatic HUDF ($22 \lesssim AB \lesssim 30$ mag; Beckwith et al. 2006; Driver et al. 2016), and references therein. The HUDF/XDF limits are indicated by the green labels in the top right corner of Fig 1a-1b. Orange labels indicate the anticipated JWST Webb Medium Deep Field (WMDF) and UltraDeep Field (WUDF) survey limits, while red indicates a Webb UltraDeep Frontier Field (WUDFF) survey limit if pointed at a gravitationally lensing Frontier Field cluster. The 5σ point source detection limits for each of these surveys are indicated in Fig. 2, and for both HST and JWST assume an effective PSF width of $0''.08$ FWHM (Windhorst et al. 2008). Blue labels indicate the anticipated 5σ point source sensitivity limit of $AB \lesssim 31$ mag of unlensed objects for ORCAS+Keck with an image PSF with $0''.01\text{--}0''.02$ FWHM at $0.5\text{--}1.2 \mu\text{m}$ wavelength. If ORCAS were to frequently monitor the best gravitational lensing clusters, we may detect compact sources intrinsically as faint as $AB \lesssim 35\text{--}36$ mag when lensed. For an HST and

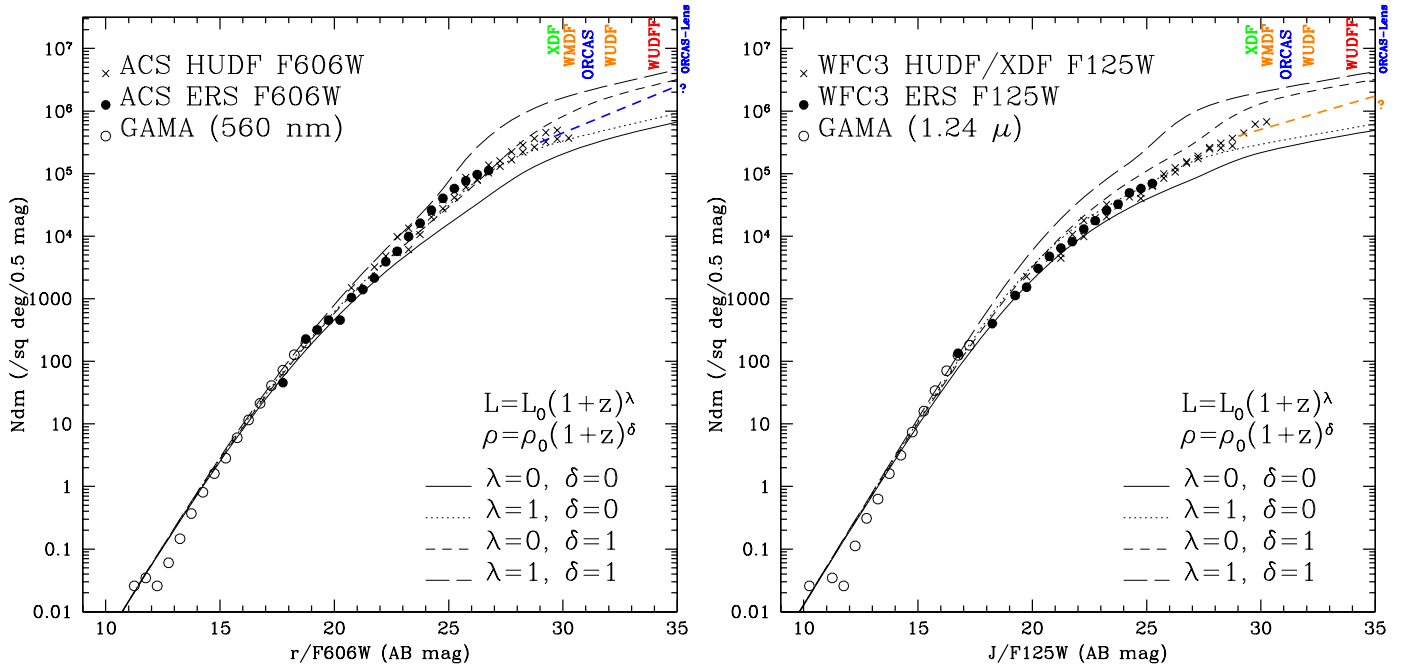


Figure 1. (a) [Left]: Differential galaxy counts in the V-band or F606W filter. Data are from the ground-based GAMA survey and the HST ACS/WFC surveys in the WFC3 ERS and HUDF fields. Combined ground-based + HST-surveys cover $10 \lesssim AB \lesssim 30$ mag (Windhorst et al. 2011; Driver et al. 2016). Simple luminosity+density evolution models are shown and extrapolated to $AB \lesssim 35$ mag (see § 2 for details). (b) [Right]: As Fig. 1a, but in the J-band or HST WFC3/IR F125W filter. The colored labels indicate the various HUDF/XDF, Webb and ORCAS detection limits without and with lensing. To $AB \lesssim 31$ mag in both filters, ORCAS will yield about 5×10^6 faint star-forming (SF) clumps per square degree, or ~ 0.4 per arcsec², or one in every box of $1.6 \times 1.6''$.

JWST PSF with $\text{FWHM} \lesssim 0''.08$, the depth increase from WUDF to WUDFF is about 2–3 mag, given the larger unlensed SF-object sizes ($\sim 0''.005$ – $0''.080$) sampled, while for ORCAS these magnifications could be ~ 3 – 4 mag for the anticipated *smaller* unlensed SF-clump sizes ($\sim 0''.001$ – $0''.080$) that it may sample (see Fig. 2).

The observed panchromatic (0.2 – $1.6 \mu\text{m}$) galaxy counts attain a converging slope ($\alpha < 0.40$) for the general flux range of $AB \simeq 17$ – 25 mag (Windhorst et al. 2011; Driver et al. 2016). These counts were fit with models that include luminosity + density evolution, as indicated by the four curves in Fig 1a-1b. Some of these models fit the panchromatic counts remarkably well for $10 \lesssim AB \lesssim 30$ mag. We use the differential count slope as a function of wavelength (Windhorst et al. 2011) to extrapolate the observed counts to the $31 \lesssim AB \lesssim 35$ mag range. At brighter fluxes, the 0.60 – $1.25 \mu\text{m}$ count-slopes are 0.30 – 0.26 mag/dex, respectively, but for $AB \gtrsim 30$ mag we adopt extrapolations with count slopes of approximately 0.15 – 0.10 dex/mag, as indicated by the blue and orange dashed lines in the upper-right corners of Fig 1a-1b. The justification for this extrapolation is that the faint-end slope of the galaxy counts is dominated by galaxies at the median redshift, which in ultradeep redshift surveys approaches the peak in the cosmic star-formation diagram at $z \simeq 1.9$ (Madau & Dickinson 2014). At this redshift, the best fit faint-end slope of the Schechter LF is $\alpha \simeq 1.4$ in linear flux units (Hathi et al. 2010; Finkelstein 2016), so when converted to a magnitude count-slope, the faint-end slope of the galaxy counts is $\gamma \simeq (1.4 - 1) / 2.5 \simeq 0.16$ dex/mag. It is possible that for fluxes fainter than $AB \sim 31$ mag the LF at $z \gtrsim 2$ — and therefore the observed counts — may turn over with a slope flatter than observed at brighter levels, but there are arguments against this too (for a discussion, see *e.g.*, §2.3 of Windhorst et al. 2018). The adopted extrapolated slopes in Fig 1a-1b are in line with the trend of the very faint-end of the plotted galaxy counts models. In both the 0.60 and $1.25 \mu\text{m}$ filters, the counts integrate to 5.0×10^6 faint star-forming (SF) clumps per square degree to $AB \lesssim 31$ mag. (To go from differential to integral counts in Fig 1a-1b, one needs to multiply the differential surface density at $AB = 31$ mag by $2 \times$ to get the counts per 1.0 -mag bin, and by $\sim 3.5 \times$ to get the total integral counts over all magnitude bins.) This surface density corresponds to ~ 0.4 SF-object per arcsec² to $AB \lesssim 31$ mag, or on average one object in every box of $1.6 \times 1.6''$. A $\gtrsim 5 \times 5''$ FOV of the ORCAS IFU may therefore provide just enough compact SF clumps to do it relative m.a.s.-astrometry as needed in, *e.g.*, § 4.

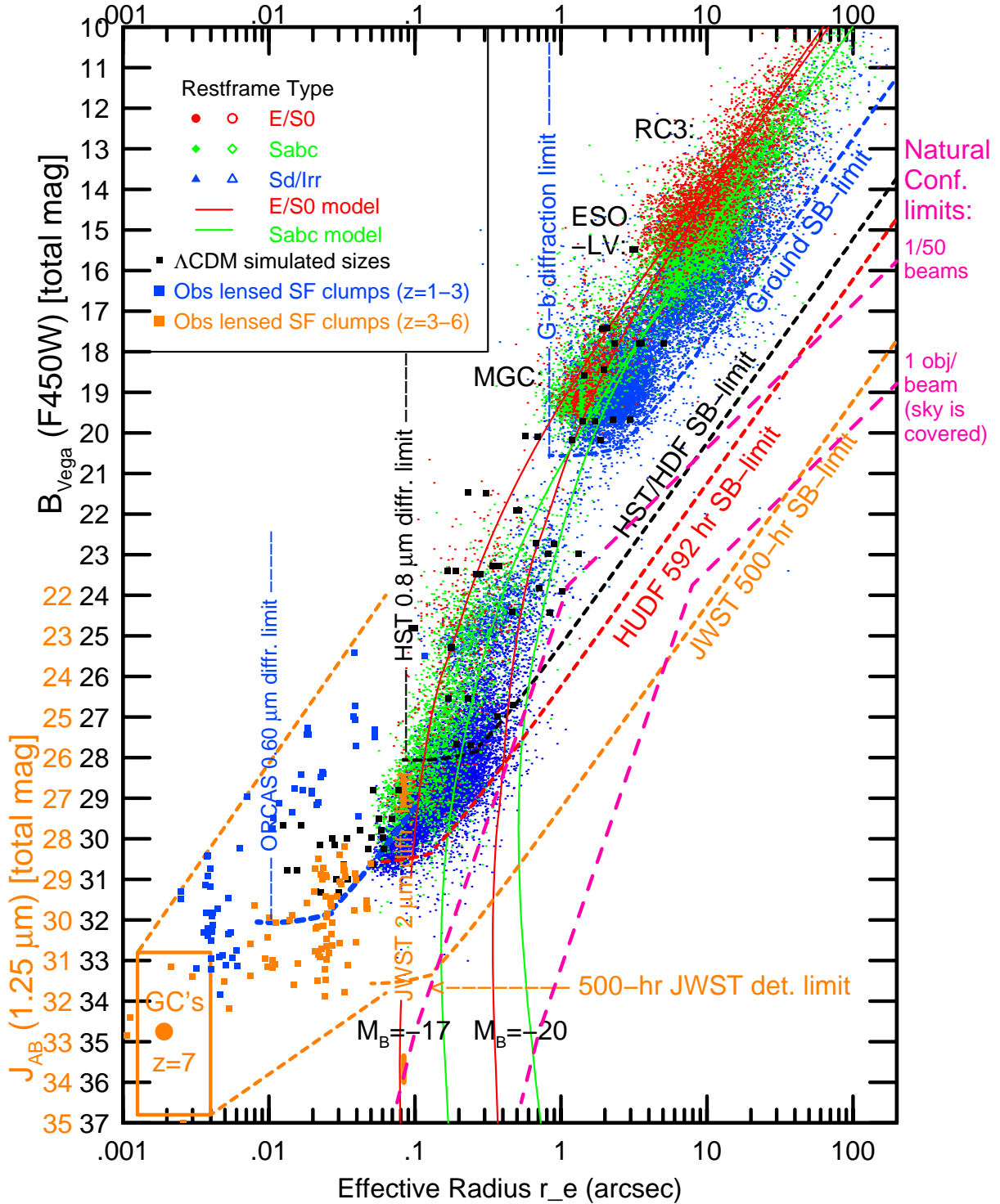


Figure 2. Galaxy sizes r_e vs. B_{Vega} or J_{AB} -magnitude from the RC3 to the HUDF limit. Short dashed lines indicate survey-limit wedges for the HDF (black), HUDF (red; in i_{AB}), and JWST (orange): diffraction limits are vertical, point-source sensitivity limits horizontal, and SB-sensitivity limits have slanted slopes = +5 mag/dex. Broken long-dashed pink lines indicate the natural confusion limit (at the level of 1 detected object per 50 “beams” or object area), to the right of which objects would begin to statistically overlap due to their own sizes and surface densities. Red and green lines indicate the expected *non-evolving* sizes for RC3 elliptical and spiral galaxies at the listed M_{AB} -values, respectively. Blue and orange squares indicate SF-clumps from gravitational lensing samples with intrinsic physical sizes converted to r_e (”), and unmagnified absolute UV-magnitudes converted to B-mag for $z=1-3$ or J_{AB} for $z=3-6$ (the J_{AB} -scale is shown approximately offset in orange for $z \geq 3$; the i_{AB} -scale is between B and J_{AB}). Black squares indicate galaxy sizes from hierarchical simulations. The orange box shows where Globular Clusters at $z=7$ are expected. For details, see § 3. Most galaxies at $J_{AB} \gtrsim 27-28$ mag are expected to be smaller than the HST and JWST diffraction limits (*i.e.*, $r_{hl} \lesssim 0''.08$). About half the faint SF-clumps to $AB \lesssim 31$ mag are expected to be (barely) resolved at the ORCAS resolution of $0''.01-0''.02$ FWHM. [Figure adapted from Windhorst et al. (2008)].

3. THE SIZE DISTRIBUTION OF FAINT STAR-FORMING CLUMPS TO $r_e \gtrsim 0''.01$ FOR ORCAS

The median sizes of faint galaxies decline steadily towards higher redshifts and also towards fainter magnitudes, as shown in Fig. 2. Red, green and blue dots show early-type, spiral, and irregular/SF galaxies respectively (*e.g.*, Odewahn et al. 1996; Cohen et al. 2003). Galaxy structural classification needs to be as much as possible done at rest-frame wavelengths longwards of the Balmer break at high redshifts too avoid caveats from the morphological K-correction (*e.g.*, Giavalisco et al. 1996; Odewahn et al. 2002; Windhorst et al. 2002; Taylor-Mager et al. 2007). Red and green lines show the best fit regression for local galaxies and its extrapolation at fixed M_{AB} -values to fainter magnitudes.

The HST/WFCP2 Hubble Deep Field (Williams et al. 1996) and the HST/ACS Hubble Ultra Deep Field Beckwith et al. (2006) showed that high redshift galaxies are intrinsically very small with typical sizes of $r_{hl} \simeq 0''.12$ or 0.7–0.9 kpc at $z \simeq 4$ –6, and sample correspondingly fainter absolute AB-magnitudes. The unique combination of these ground-based and HST surveys shows that the apparent galaxy sizes decline steadily from the RC3 to the HUDF limits (Windhorst et al. 2008, and Fig. 2 here). Most galaxies at $J_{AB} \gtrsim 28$ mag are thus likely unresolved at $r_{hl} \lesssim 0''.1$ FWHM, as suggested by galaxy sizes from hierarchical simulations (black squares in Fig. 2; Kawata et al. 2004).

SB and other selection effects in these surveys are significant. For each survey, the diffraction limit for point sources is shown as vertical dashed line with the survey indicated, while the nearly horizontal line of the same color indicates for each survey the corresponding $\sim 5\sigma$ point-source sensitivity, and the slanted dashed line (with a slope of 5 mag/dex) indicates that survey’s corresponding SB-sensitivity. That is, each survey cannot detect objects outside this wedge-shaped area. The pink lines indicate the natural confusion limit discussed in Windhorst et al. (2008), that were derived from the (assumed broken power-law) counts in Fig. 1a–1b. As opposed to the instrumental confusion limit, which is determined by the FWHM of the PSF in each survey, the natural confusion lines indicate the region where galaxies would be large enough that their effective area, πr_e^2 or “the galaxy beam”, would occupy more than 1/50 of the total survey area, thereby limiting the ability of source detection and deblending algorithms to provide complete catalogs of overlapping objects. This is primarily visible for galaxies in the HDF and HUDF for $24 \lesssim B \lesssim 28$ mag and $0''.4 \lesssim r_e \lesssim 0''.8$, where samples become incomplete as they are no longer bunching up against the SB-selection lines. Natural confusion is expected to become more significant for JWST surveys when they are pushed to fainter than $AB \simeq 30$ –31 mag.

Extensive recent studies with HST of several of the best lensing clusters have resulted in many SF clumps at $z \simeq 1$ –6.6 that are observed close to the critical curves, where they appear highly gravitationally stretched and highly magnified in their total flux (*e.g.*, Lotz et al. 2017; Johnson et al. 2017a,b; Vanzella et al. 2021). Of particular importance are the VLT MUSE spectra and redshifts that have been obtained for many of these SF clumps (Vanzella et al. 2019, 2021), which are shown in Fig. 2 as the blue ($z \simeq 1$ –3) and orange ($z \simeq 3$ –6.6) squares at their *intrinsic* (*i.e.*, unlensed) physical sizes and *unmagnified* absolute magnitudes (*i.e.*, their observed M_{AB} -values after dividing by their lensing magnification). In Fig. 2 their unlensed physical sizes were converted to r_e in arcsec, and their unmagnified M_{UV} -values were converted to B- or J_{AB} -magnitudes at the corresponding redshifts in Λ CDM cosmology. Volume completeness is always hard to estimate even for these best available gravitational lensing surveys with faint object spectroscopy, but at least these objects show up in significant numbers in these surveys, and they populate the *unmagnified flux range* of $24 \lesssim AB \lesssim 34$ mag, and the *intrinsic, unlensed size range* of $0''.001 \lesssim r_e \lesssim 0''.08$ in Fig. 2. About half of these SF clumps are expected to be visible down to the ORCAS diffraction limit, while the other half will be slightly resolved, but still mostly above the ORCAS SB-limits. A $\gtrsim 5 \times 5''$ ORCAS FOV may therefore provide just enough compact SF clumps to do relative (sub-)m.a.s.-astrometry, depending on the S/R-ratio achieved, which is needed in § 4.

Natural confusion is expected to be less important for ORCAS+Keck, since the sampled unlensed SF-clump sizes from the HST gravitational lensing samples are much smaller than the HST diffraction limit. Yet is it possible that a number of larger SF clumps will fall below the ORCAS SB-limits, and only more hierarchical simulations (black squares) and deeper ORCAS observations will be able to assess this more precisely.

4. MONITORING CAUSTIC TRANSITS OF EARLY STARS WITH ORCAS

Cluster caustic transits can occur when a compact restframe UV source transits a caustic due to the transverse cluster motion in the sky, or perhaps due to significant velocity substructure in the cluster, and have the great potential of magnifying such compact objects temporarily by factors of $\mu \simeq 10^3$ – 10^5 (*e.g.*, Miralda-Escude 1991). This is because: (1) the clusters and their substructures may have transverse motions as high as $v_T \lesssim 1000$ km s $^{-1}$, (2) stars at $z \simeq 1$ –7 (including population III stars at $z \gtrsim 7$) have radii $R \simeq 1$ –10 R_\odot , and (3) in the source plane the main caustic magnification goes as: $\mu \simeq 10 \cdot (d_{caustic}/'')^{-1/2}$, where $d_{caustic}$ is the distance of the star to the cluster caustic in arcsec.

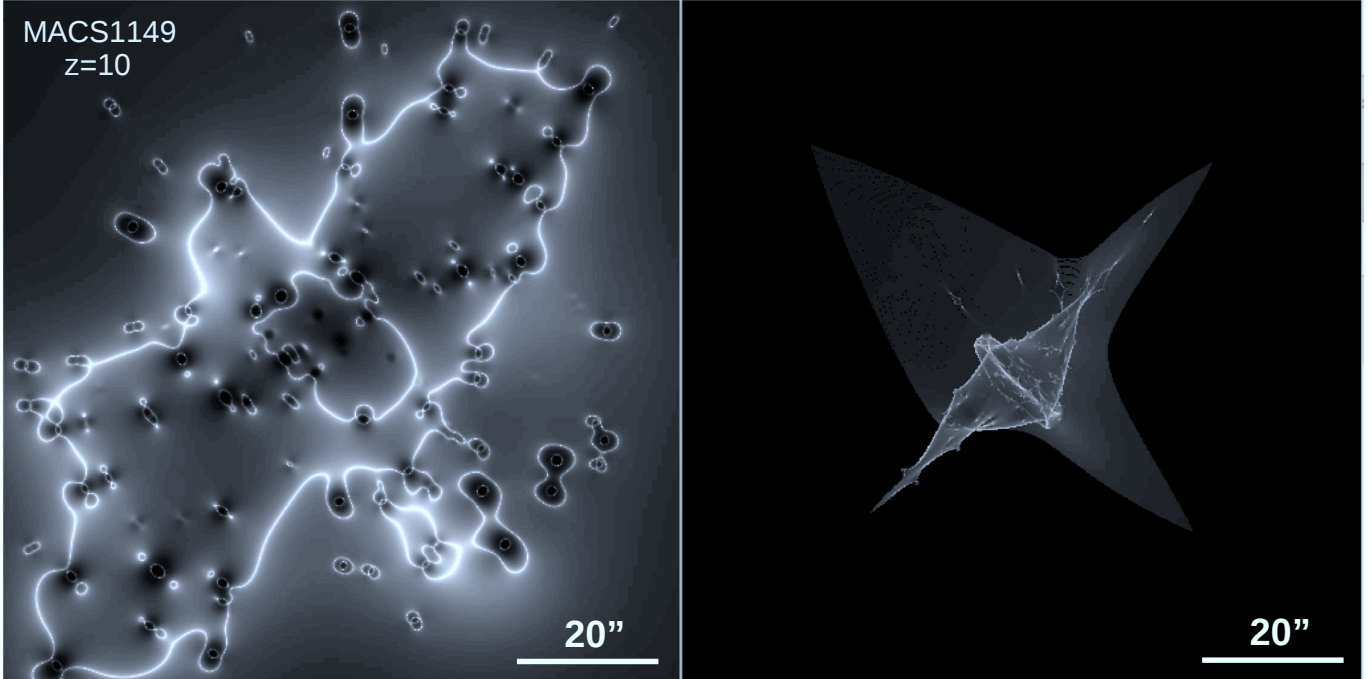


Figure 3. [LEFT] Example of the lensing magnification map for galaxy cluster MACS J1149.5+2223 at $z \simeq 0.54$ and a background source at $z=10$ (e.g., Lotz et al. 2017, and references therein). Light from the cluster galaxies is not shown to avoid overcrowding, but can be found in those papers. The white areas mark the critical curves, where maximum lensing magnification is observed from this cluster for a background source with half-light radius $r_{\text{hl}} \lesssim 0''.5$ at $z=10$. The lightest regions have the highest magnification ($\mu \gtrsim 10\text{--}20$), while the darkest regions are areas of low magnification ($\mu \simeq 1$ or even $\mu \lesssim 1$) around the cluster member galaxies. [RIGHT] Caustic map produced by the cluster mass model for a background source at $z=10$. This is the location where a point source at $z=10$ produces maximum magnification. The total length of the cluster caustics is $L \simeq 100''$ when estimating caustic transit probabilities (for details, see § 4 and Windhorst et al. 2018).

This is illustrated in Fig. 3 as reproduced from Windhorst et al. (2018). Since stars at $z \gtrsim 7$, including Pop III stars, are of order $\sim 10^{-11}$ arcsec across at $z \simeq 1\text{--}17$, such caustic transits could temporarily boost the brightness of a very compact object by $\mu \simeq 7.5\text{--}12.5$ mag, which may render it observable by JWST (e.g., Windhorst et al. 2018) and also ORCAS+Keck. The best lensing clusters are typically at $z \simeq 0.3\text{--}0.5$, and are by selection the most massive, largely virialized clusters. Lensing clusters with some significant velocity substructure are preferred, since they tend to have more significant transverse motions that increase the likelihood of caustic transits.

In the absence of microlensing by faint stars in the cluster IntraCluster Light (ICL), these caustic transits may boost the apparent magnitude of these stars by $\mu \simeq 7.5\text{--}12.5$ mag for several months. This has been observed with HST for a number of hot (OB-type) stars at $z \simeq 1\text{--}1.5$ (Kelly et al. 2017b; Diego et al. 2018; Rodney et al. 2018; Venumadhav et al. 2017; Chen et al. 2019; Kaurov et al. 2019). Windhorst et al. (2018) calculated the frequency of such events from both MESA models for Pop III stars and multicolor accretion disks for stellar mass black holes at $z \simeq 7\text{--}17$. Both will have roughly the same radii ($R \simeq 1\text{--}100 R_{\odot}$) and effective temperatures ($T_{\text{eff}} \sim 50,000\text{--}100,000$ K), since they will radiate close to the Eddington limit, and therefore they will have similar rest-frame UV SB. (The only difference is that Pop III stars never get much hotter than 105,000 K, while stellar mass black hole accretion disks will also radiate in X-rays when fed from lower mass companion stars in their AGB stage). Microlensing by faint foreground stars in the cluster ICL would dilute the macrolensed signal across the main caustic somewhat, but could also spread it out over more peaks over a longer period of time (Diego et al. 2018). The resulting expectation is that JWST may observe such events at the rate of up to ~ 0.3 per cluster per year if the best lensing clusters are monitored a few times each year with JWST NIRCcam (Windhorst et al. 2018).

While the ORCAS FOV is too small for a blind survey of caustic transits at $z \gtrsim 1$, it is of particular interest to follow up with ORCAS on caustic transits of individual stars in SF clumps at $z \gtrsim 1\text{--}2$ that have been detected with HST, and on caustic transits that may be detected with JWST at $z \simeq 6\text{--}17$ at extreme magnifications ($\mu \gtrsim 10^3\text{--}10^5$) for the first stars and their stellar mass black hole accretion disks. The ability for ORCAS to monitor such objects for

decades across the (micro-)caustics provides a unique opportunity to obtain a statistical census of individual stars at cosmological distances. For instance, one could use different ORCAS epochs to precisely estimate the centroid position of a lensed star that is very close to a caustic. Assuming the two counter images of the star would form an unresolved duplet with a separation of less than the ORCAS resolution, microlensing in each of the two counter images could make the centroid of the observed image shift from epoch to epoch (*e.g.*, Diego 2019), which ORCAS could monitor at high precision. This then would add a powerful time-domain constraint to gravitational lensing models, in addition to the constraints provided by very deep high-resolution imaging.

5. SUMMARY OF SCIENCE GOALS AND ORCAS REQUIREMENTS

Here we summarize the ORCAS science goals on faint SF-clumps and their implications for the ORCAS Requirements Matrix as following. Note that Science Goal 1+2 may be achieved from other random ORCAS imaging of very faint foreground targets, such as solar system KBO's:

Science Goal 1: Constrain the number densities of the faintest SF-clumps at $z \simeq 1-7$. ORCAS will address how galaxies assemble from smaller clumps to stable disks by measuring ages, metallicities, and gradients of clumps within galaxies.

Requirements 1:

- Deep images to $AB \lesssim 31$ mag for point sources in a few hours, necessary to sample SF-clumps with a surface density of 5.0×10^6 per square degree.
- An $\gtrsim 5 \times 5''$ FOV (that includes IFU capabilities), which at 5.0×10^6 objects per square degree will contain ~ 10 faint SF clumps. This is a minimum needed to do *relative* (sub-)m.a.s.-astrometry, depending on the S/R-ratio achieved, and anticipating that most objects will be compact enough to auto-correlate their images to get the best possible relative astrometric positions.
- Wavelength coverage ideally at 0.3–2.2 μm , but at minimum 0.5–1.2 μm . Standard ugriz+YJHK filter set with potential modifications suggested below and in Fig. 4, to get photometric redshift estimates before IFU spectroscopy is attempted. IFU follow-up on selected targets will be needed.
- At minimum 10 ORCAS fields would be needed to start a census for ~ 100 of these faint SF clumps. A long term goal should be to get at least 100 ORCAS fields to get a more accurate assessment of the redshift, luminosity and size distribution from ~ 1000 SF clumps.

Science Goal 2: Constrain the physical sizes of the faintest SF-clumps at $z \simeq 1-7$. Anticipated typical angular sizes at $z \simeq 1-7$ are $r_e \simeq 1-80$ m.a.s. to $AB \lesssim 31$ mag. About half of these SF clumps will be below the ORCAS diffraction limit, and the other half will be slightly resolved, but still mostly above the ORCAS surface brightness (SB) limits.

Requirements 2:

- Spatial resolution of $\sim 0''.01-0''.02$ FWHM, with good Strehl ratios.
- If SB-sensitivity for the larger SF-clumps becomes an issue, ORCAS should consider some “notch-filters”, as shown in Fig. 4.

Science Goal 3: Follow up with ORCAS on caustic transits of individual stars in SF clumps at $z \gtrsim 1-2$ that have been detected with HST, and those that may be detected with JWST at $z \simeq 6-17$ at extreme magnifications ($\mu \gtrsim 10^3-10^5$) for the first stars and their stellar mass black hole accretion disks.

Requirements 3:

- Deep images to $AB \lesssim 31$ mag for point sources. Unmagnified magnitudes (*i.e.*, their observed lensed fluxes after dividing by their lensing magnification) may be as faint as $AB \lesssim 35-36$ mag.
- Spatial resolution of $\sim 0''.01-0''.02$ FWHM. Unlensed sizes may be smaller than 1–10 m.a.s. when searching with ORCAS around the critical curves of the best lensing galaxy clusters imaged with HST and JWST.
- *Relative* (sub-)m.a.s.-astrometry will be needed to monitor potential parity changes of lensed sources when they go across a caustic, and therefore may change shape or apparent position at high redshift (Note: this is not a true proper

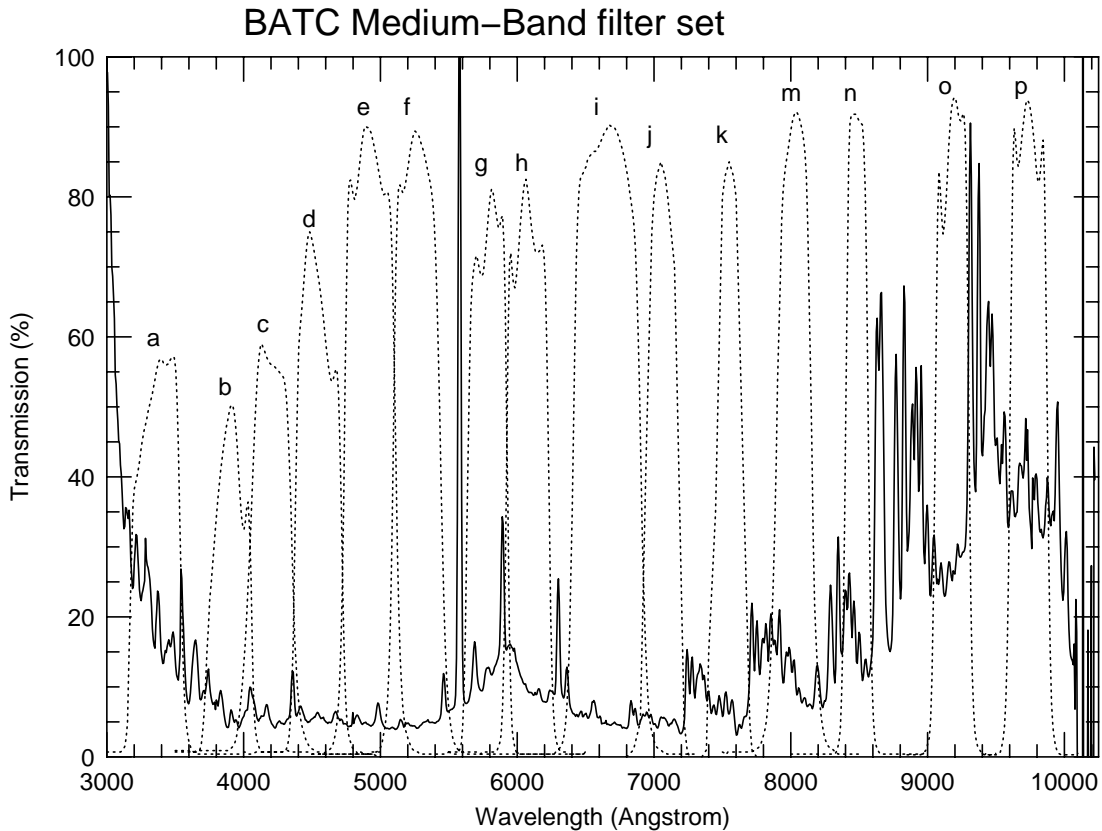


Figure 4. An example of medium-band filters that avoid most of the brightest night-sky lines affecting ground-based observations (Yan et al. 2000). ORCAS will likely mostly target very faint objects, possibly in a standard broad-band filter set like ugriz+YJHK. More than half of these objects may be slightly resolved at ORCAS’ spatial resolution of $0''.01$ – $0''.02$ FWHM (Fig.2). Hence, to maximize the SB-sensitivity for the very faintest slightly resolved objects, ORCAS could consider replacing some of the broad-band filters that include the brightest night-sky lines with “notch-filters” that essentially suppress these lines. E.g., one could replace the V-band or F606W filter with a notch-filter that consist of filter $f+g$ or $g+h$ here. This would permit imaging to lower SB-levels (e.g., Shang et al. 1998).

motion, but a light-path change of the lensed source in the gravitational landscape of the lensing cluster when the source goes across a caustic.

- Monitor caustic-transiting stars for decades across the (micro-)caustics to obtain a statistical census of individual stars at cosmological distances, and the microlensing stellar population in the foreground galaxy cluster ICL.
- Preimaging with HST or follow-up imaging with JWST of ORCAS targets may be needed to identify the best possible candidates for caustic transits.

REFERENCES

- Abraham, R. G., Tanvir, N. R., Santiago, B. X., et al. 1996, MNRAS, 279, L47
- Allen, R. J., Kacprzak, G. G., Glazebrook, K., et al. 2017, ApJ, 834, L11
- Beckwith, S. V. W., Stiavelli, M., Koekemoer, A. M., et al. 2006, AJ, 132, 1729
- Bouwens, R. J., Illingworth, G. D., Thompson, R. I., et al. 2004a, ApJ, 606, L25
- Chen, W., Kelly, P. L., Diego, J. M., et al. 2019, ApJ, 881, 8
- Cohen, S. H., Windhorst, R. A., Odewahn, S. C., et al. 2003, AJ, 125, 1762
- Cristiani, S., Renzini, A., & Williams, R. E. 2001, ESO Astroph. Symp. (Berlin: Springer-Verlag), ISBN 3-540-42799-6
- Diego, J. M., Kaiser, N., Broadhurst, T., et al. 2018, ApJ, 857, 25 (astro-ph/1706.10281)
- Diego, J. M. 2019, A&A, 625, A84.
- Driver, S. P., Windhorst, R. A., Ostrander, E. J., et al. 1995, ApJ, 449, L23

- Driver, S. P., Fernández-Soto, A., Couch, W. J., et al. 1998, *ApJ*, 496, L93.
- Driver, S. P., Hill, D. T., Kelvin, L. S., et al. 2011, *MNRAS*, 413, 971.
- Driver, S. P., Andrews, S. K., Davies, L. J., et al. 2016, *ApJ*, 827, 108 (D16)
- Ellerbroek, B. L. & Bonaccini Calia, D. 2006, *SPIE Vol.* 6272,
- Elmegreen, D. M., Elmegreen, B. G., Ravindranath, S., & Coe, D. A. 2007, *ApJ*, 658, 763
- Ferguson, H. C., Dickinson, M., Giavalisco, M., et al. 2004, *ApJ*, 600, L107
- Finkelstein, S. L. 2016, *PASA*, 33, e037
- Fisher, D. B., Glazebrook, K., Abraham, R. G., et al. 2017, *ApJL*, 839, L5
- Fisher, D. B., Glazebrook, K., Damjanov, I., et al. 2017, *MNRAS*, 464, 491
- Gardner, J. P., Mather, J. C., Clampin, M., et al. 2006, *Space Science Res.*, Vol. 123, 485
- Giavalisco, M., Livio, M., Bohlin, R. C., et al. 1996, *AJ*, 112, 369
- Giavalisco, M., Ferguson, H. C., Koekemoer, A. M., et al. 2004, *ApJ*, 600, L92
- Glazebrook, K., Ellis, R., Sanriago, B., & Griffith, R. 1995, *MNRAS*, 275, L19
- Griffiths, R. E., Casertano, S., Ratnatunga, K. U., et al. 1994, *ApJ*, 435, L19
- Grogin, N. A., Kocevski, D. D., Faber, S. M., et al. 2011, *ApJS*, 197, 35
- Hathi, N. P., Jansen, R. A., Windhorst, R. A., et al. 2008, *AJ*, 135, 156
- Hathi, N. P., Ryan, R. E., Cohen, S. H., et al. 2010, *ApJ*, 720, 1708
- Johnson, T. L., Rigby, J. R., Sharon, K., et al. 2017, *ApJL*, 843, L21
- Johnson, T. L., Sharon, K., Gladders, M. D., et al. 2017, *ApJ*, 843, 78
- Kaurov, A. A., Dai, L., Venumadhav, T., et al. 2019, *ApJ*, 880, 58
- Kawata, D., Gibson, B. K., & Windhorst, R. A. 2004, *MNRAS*, 354, 387,
- Kelly, P. L., Diego, J. M., Rodney, S., et al. 2018, *Nature Astr.*, 2, 334 (astro-ph/1706.10279)
- Koekemoer, A. M., Faber, S. M., Ferguson, H. C., et al. 2011, *ApJS*, 197, 36
- Lilly, S., Schade, D., Ellis, R., et al. 1998, *ApJ*, 500, 75
- Lilly, S. J., Le Fèvre, O., Renzini, A., et al. 2007, *ApJS*, astro-ph/0612291
- Livio, M., Fall, S. M., & Madau, P. 1998, *STScI Symp. Series No. 11* (New York: Cambridge University Press)
- Lotz, J. M., Koekemoer, A., Coe, D., et al. 2017, *ApJ*, 837, 97
- Madau, P., & Dickinson, M. 2014, *ARA&A*, 52, 415
- Mather, J. C., MacEwen, H.A. & de Graauw, M. W. M. 2006, “Space Telescopes and Instrumentation I: Optical, Infrared, and Millimeter” *SPIE Vol.* 6265
- McDermid, R. M., Cresci, G., Rigaut, F., et al. 2021, astro-ph/2009.09242
- Miralda-Escude, J. 1991, *ApJ*, 379, 94
- Navarro, J. F., Frenk, C. S., & White, S. D. M. 1996, *ApJ*, 462, 563
- Odehahn, S. C., Windhorst, R. A., Driver, S. P., & Keel, W. C. 1996, *ApJ*, 472, L13
- Odehahn, S. C., Cohen, S. H., Windhorst, R. A., & Philip, N. S. 2002, *ApJ*, 568, 539
- Pascarelle, S. M., Windhorst, R. A., Keel, W. C., & Odehahn, S.C. 1996, *Nature*, 383, 45
- Rigby, J. R., Johnson, T. L., Sharon, K., et al. 2017, *ApJ*, 843, 79
- Rix, H.- W., Barden, M., Beckwith, S. V. W., et al. 2004, *ApJS*, 152, 163
- Rodney, S. A., Balestra, I., Bradac, M., et al. 2018, *Nature Astr.* 2, 324
- Scoville, N., Aussel, H., Brusa, M., et al. 2007, *ApJS*, 172, 1
- Shang, Z., Zheng, Z., Brinks, E., et al. 1998, *ApJL*, 504, L23
- Taylor-Mager, V. A., Conselice, C. J., Windhorst, R. A., & Jansen, R. A. 2007, *ApJ*, 659, 162
- Vanzella, E., Calura, F., Meneghetti, M., et al. 2019, *MNRAS*, 483, 3618
- Vanzella, E., Caminha, G. B., Calura, F., et al. 2020, *MNRAS*, 491, 1093
- Vanzella, E., Caminha, G. B., Rosati, P., et al. 2021, *A&A*, 646, A57
- Venumadhav, T., Dai, L., & Miralda-Escudé, J. 2017, *ApJ*, 850, 49
- Williams, R. E., Blacker, B., Dickinson, M., et al. 1996, *AJ*, 112, 1335
- Windhorst, R. A., Taylor, V. A., Jansen, R. A., et al. 2002, *ApJS*, 143, 113
- Windhorst, R. A., Hathi, N. P., Cohen, S. H., et al. 2008, *Advances in Space Research*, 41, 1965
- Windhorst, R. A., Cohen, S. H., Hathi, N. P., et al. 2011, *ApJS*, 193, 27 (astro-ph/1005.2776)
- Windhorst, R. A., Timmes, F.X., Wyithe, J. S. B., et al. 2018, *ApJS*, 234, 41 (astro-ph/1801.03584)
- Yan, H., Burstein, D., Fan, X., et al. 2000, *PASP*, 112, 691
- Yan, H., & Windhorst, R. A. 2004b, *ApJ*, 612, L93